JOTCS A
Journal of the Turkish Chemical Society
Section: A
Chemistry
TURKISH CHEMICAL SOCIETY

DFT Calculations of Trilayer Heterostructures from $MoSe_2$, PtS_2 Monolayers in Different Orders with Promising Optoelectronic Properties

Jassim M. Al-Issawe[1], Idrees Oreibi[1,*]

[1]Directorate of Education Babylon, Ministry of Education, Iraq

Abstract: Van der Waals (vdW) heterostructures have taken the dominant place in commercialization of the optoelectronic devices. $MoSe_2$ and PtS_2 are two-dimensional semiconductors, Using first-principles computations, the optical and electronic characteristics of trilayer van der Waals (vdW) heterostructures with four distinct orders were investigated. We demonstrate that all innovative heterostructures investigated are semiconductors. In addition, it should be emphasized that the indirect band gaps of the ABA, BAA, ABB, and BAB orders (where A is $MoSe_2$ and B is PtS_2) are approximately 0.875, 0.68, 0.595, and 0.594 eV, respectively. Positively, the optical characteristics reveal that the trilayer heterostructures strongly absorb light with energies ranging from infrared to ultraviolet. Therefore, these heterostructures can be utilized in optoelectronic devices in these regions.

Keywords: DFT, heterostructures, trilayer, optoelectronic

Submitted: May 11, 2023. **Accepted:** December 26, 2023.

Cite this: Al-Issawe JM, Oreibi I. DFT Calculations of Trilayer Heterostructures from MoSe2, PtS2 Monolayers in Different Orders with Promising Optoelectronic Properties. JOTCSA. 2024; 11(2): 405-14.

DOI: https://doi.org/10.18596/jotcsa.1295960.

***Corresponding author. E-mail:** idrees114af@gmail.com

1. INTRODUCTION

Shortly after the discovery of graphene, two-dimensional (2D) materials became the focus of material research (1). The effectiveness of using graphene in nanotechnology and nanodevices has started a thorough investigation and study into layered low-dimensional materials (2). Graphene has spurred substantial research into two-dimensional (2D) materials such as TMDs (3), silicene (4), MXY Janus (5), germanene (6), III-group monochalcogenides (7, 8), phosphorene (9), and stanene (10).

Vertical heterostructures comprised of transition metal dichalcogenides (TMDs) monolayers are attractive prospects for next-generation optoelectronic and thermoelectric devices (11). These materials are more adaptable as candidates for thin, flexible device applications and are beneficial for numerous applications, including photovoltaic devices (12, 13), transistors (14), Electrochemical Energy Systems (15, 16), lubrication (17, 18), lithium-ion batteries (16, 19), optoelectronic nanodevices (20), and thermoelectric devices (21). Transition metal dichalcogenide (TMDs) semiconductors and their bi-layer/tri-layer heterostructures have attracted significant attention because of their rich electronic/photonic properties such as a high carrier mobility (22), indirect to direct band gap transition (23), and abundance of multiexcitons (24), as well as importance for fundamental research and novel device applications (25, 26). TMDs monolayers are the most researched 2D semiconductors, with substantial exciton states and accessibility to the valley degree of freedom (27). TMDs materials are atomically 2D MX2 semiconductors of the type MX_2, with M a transition metal atom (Mo, W, etc.) and X a chalcogen atom (S, Se, or Te), Many of these materials have been made in the laboratory, such as MoS2 (28, 29), $MoSe_2$ (30), $GeSe_2$ (31), PtS_2 (32), $MoTe_2$ (33), and

WS_2 (34)...etc. Specifically, PtS_2 and $MoSe_2$ monolayers, among other TMDs materials, have become a focus of study in recent years due to their remarkable features, which make them ideal materials for transistors (35, 36), solar energy applications (37), and electrocatalysts (38). PtS_2 monolayer is a semiconducting material with a bandgap of about 1.7 eV (39). On the other hand, $MoSe_2$ monolayer is also a semiconducting material with a bandgap of about 1.5 eV (40).

Moreover, to my knowledge, no investigation into the optical and band structure characteristics of trilayer vdW heterostructures has ever been published. We shall thus study these characteristics of trilayer vdW heterostructures. The density functional theory was utilized to examine the optoelectronic characteristics of the heterostructures composed of three monolayers of PtS_2 and $MoSe_2$. Because the orders that form in the heterostructures may have a significant influence in determining the properties of the heterostructures, the examined properties are studied with four orders of trilayer vdW heterostructures. Our research could lead to a material that could be used to make optoelectronic devices.

2. COMPUTATIONAL METHODS

In this study, we calculate the optical and electronic properties of the trilayer heterostructures by first-principles calculations using castep code (41), with the generalized gradient approximations (GGA) (42). In the current work, the exchange-correlation energy function developed by Perdew, Burke, and Ernzerhof (PBE) has been applied. The interaction of valence electrons is defined by the ultrasoft pseudopotential (43). The cutoff energy for plane-wave basis was taken to be 500 eV. The 4×4×1 supercell is the model system used in this work to replicate the heterostructure, The relativistic treatment follows out via the function of Koelling-Harmon. The self-consistent energy tolerance in the calculations was deemed to be converged at 4×10^{-6} eV/atom, while the force's convergence threshold was established at 1.5×10^{-2} eV/Å. A vacuum gap of 25 Å along the perpendicular direction to the surface was utilized to exclude the interaction between two adjacent layers. To compute the geometry optimization and optical characteristics, respectively, the Brillouin zone is integrated with a 12×12×1 and 30×30×1 Monkhorst-Pack k-point mesh (44).

3. RESULTS AND DISCUSSION

3.1. Structural and Electronic Properties

Fig. 1 shows the geometrical atomic structures of $MoSe_2$ and PtS_2 monolayers from various angles. At equilibrium, $MoSe_2$ and PtS_2 monolayers correspond to the space group P-6m2 and P-3m1, respectively. the lattice constant of the single-layer $MoSe_2$ is a = b = 3.29 Å, c = 18.25 Å and the length of Mo-Se (d) is 2.522 Å, while the lattice constant of the single-layer PtS_2 is a = b = 3.58 Å, c = 17.56 Å and the length of Pt-S (d) is 2.418 Å, These results are in good agreement with previous experimental and theoretical data (45-49).

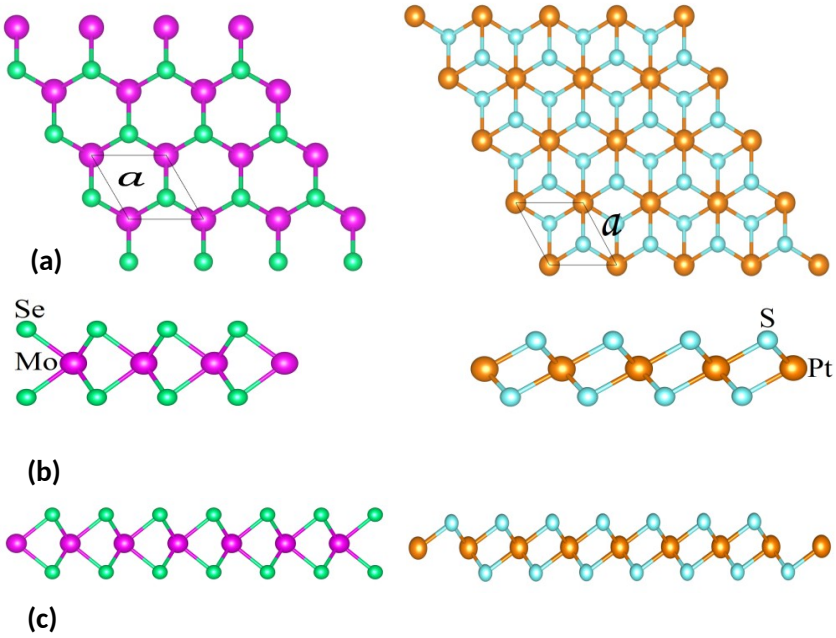

Figure 1: The top (a), side (b), and front(c) views of $MoSe_2$ and PtS_2 monolayers.

The three-layer heterostructures include four different arrangements where the monolayers are arranged perpendicular in the z-direction. These arrangements are; ABA, AAB, ABB, and BAB (where A is $MoSe_2$ and B is PtS_2) as shown in Fig. 2. The calculated interlayer distances (h), lattice constants

(a), bond lengths (d), formation energy, and bind energy have been summarized in Table 1. These values are comparable with the mean value of monolayers $MoSe_2$ and PtS_2. Our findings suggest that the arrangement of trilayer heterostructures has a significant effect on structural properties. The formation and bind energies were calculated to identify the stability of ABA, BAA, ABB, and BAB orders. Manifestly, all the formed orders are stable due to their possessing formation energies with negative values.

Table 1: The computed structural and electronic properties of trilayer heterostructures.

Orders	a=b(Å)	h_1(Å)	h_2(Å)	$D_{Mo\text{-}Se}$ (Å)	$D_{Pt\text{-}S}$ (Å)	Formation energy(eV)	binding energy (eV)
ABA	3.387	3.928	4.258	2.544	2.385	-20.43	0.47
BAA	3.385	4.005	3.976	2.729	2.385	-20.41	0.49
ABB	3.491	4.391	4.240	2.570	2.4	-18.33	0.57
BAB	3.489	4.388	4.104	2.571	2.4	-18.31	0.58

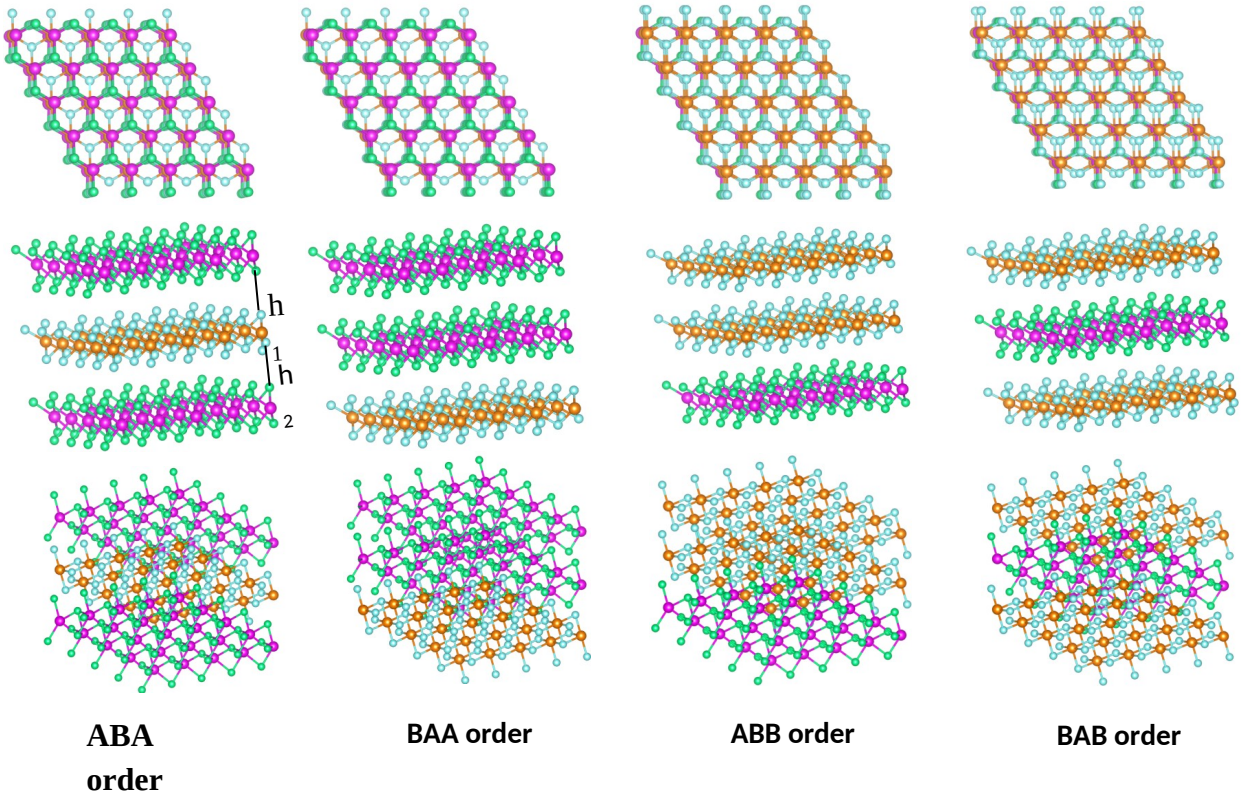

Figure 2: Atomic structures of trilayer heterostructures by different orders where A and B are $MoSe_2$ and PtS_2, respectively.

The calculations of band structure show that the $MoSe_2$ monolayer has a direct bandgap (1.489 eV) lying at Γ point and is very comparable with previous experimental data (50, 51). On the other hand, the PtS_2 monolayer having the properties of a semiconductor with indirect bandgap (1.776 eV), the conduction band minimum (CBM), and valence band maximum (VBM) placed in the Γ-M and K-Γ paths, respectively, as exhibited in Fig. 3. This result is found to be in a very good agreement with previous reports (46, 52).

Figure 4 shows the phonon dispersion of the trilayer heterostructures. We note that the BAA order is the most dynamically stable, as it is devoid of any negative values, unlike the ABA order, which shows one branch that shows negative values that may indicate instability or numerical noise. As for the ABB and BAB orders, we notice that there are few negative values at Γ, which is mostly due to numerical noise.

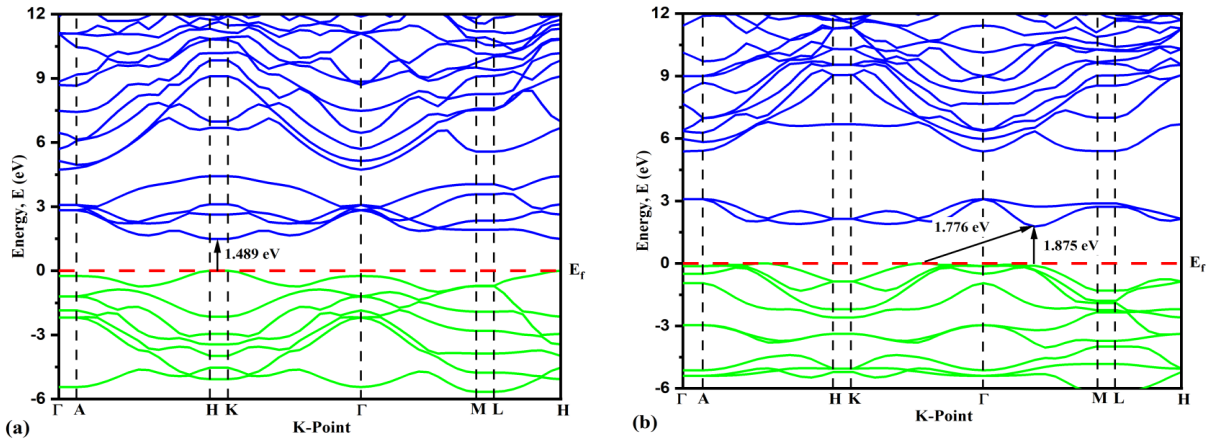

Figure 3: The band structure of the monolayers (a)$MoSe_2$, (b)PtS_2.

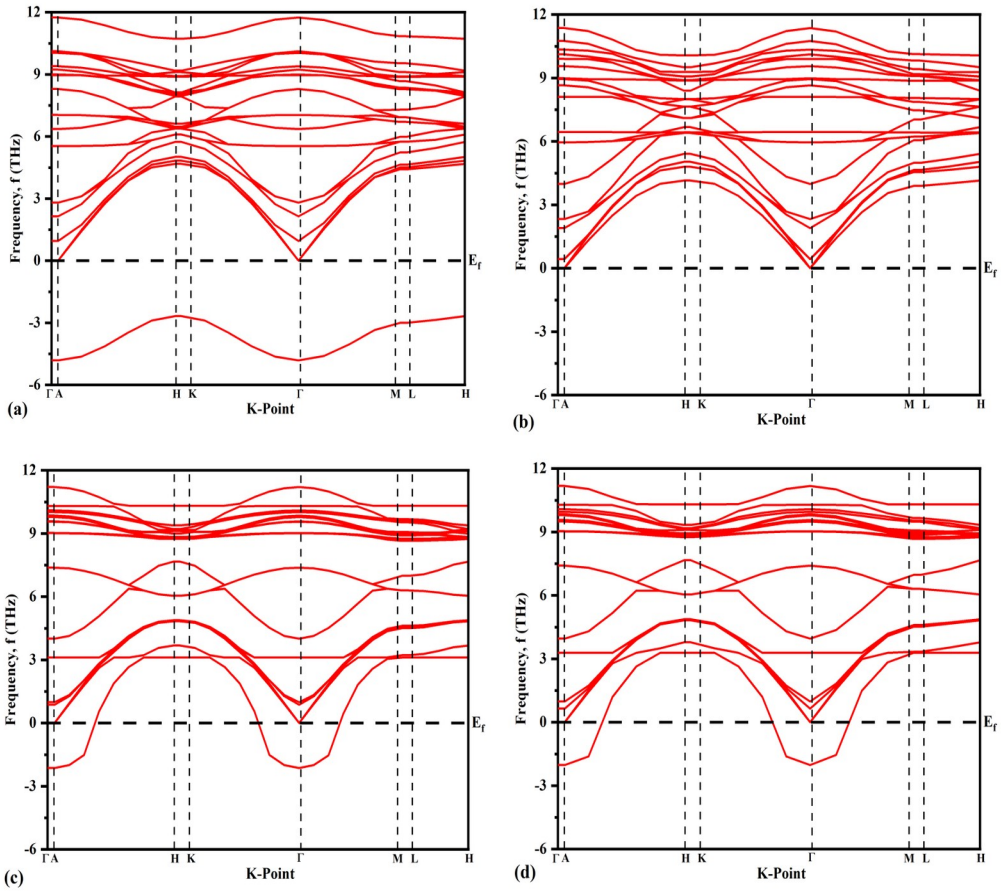

Figure 4: Phonon dispersions of trilayer heterostructures (a) ABA, (b) BAA, (c) ABB, (d) BAB orders.

Figure 5 depicts the band structure of trilayer heterostructures. The bandgaps are 0.875 eV (ABA), 0.68 eV (BAA), 0.595 eV (ABB), and 0.594 eV (BAB). These values are corresponded to the wavelengths, 1416.96 nm, 1823.29 nm, 2083.77 nm, and 2087.27 nm, respectively. From the band structure of ABA, BAA, ABB, and BAB orders, it can be seen that ABA and BAA orders have a lot in common when it comes to their direct and indirect energy gaps. The same is true for ABB and BAB orders. It should be pointed out that the VBM for all trilayers is positioned at Γ point whereas CBM is placed in (ABA and BAA) ABB and BAB orders at (K-Γ path) Γ path. However, the sites of VBM are unchanged irrespective of the heterostructure order in contrast to CBM, which depends on the heterostructure type. Although the values of bandgaps of ABB and BAB heterostructures are very comparable, the values are much smaller than those in $MoSe_2$ and PtS_2 monolayers counterparts. More precisely, the construction of trilayer heterostructures reduces the energy gap to nearly a third of its value. In another

development, there a direct bandgaps for ABA, BAA, ABB, and BAB orders are positioned at Γ path with comparable values; 1.22, 1.16, 1.013, and 1.014 eV, respectively. This indicates that the values of the direct bandgap are approximately twice the indirect bandgap. Based on these values, we can unambiguously deduce that the bandgaps are situated in the infrared (IR) range. These findings revealed that there is a high probability of utilizing heterostructures as promising materials as photovoltaic devices.

This suggests that controlling the number and arrangement of the monolayers to form the triple layers leads us to obtain a band structure with different energy gaps. This is the important feature of the triple layers that make them preferable to the monolayers that are involved in their formation. In addition, we computed the total and partial densities of state (TDOS and PDOS), and the results are shown in Fig. 6, It can be observed that the valence band (VB) and conduction band (CB) near the Fermi level (near zero) are composed of the p orbitals of sulfur and selenium atoms and the d orbitals of molybdenum and platinum atoms. The far region (-12 to -15 eV) of the valence band (VB) is dominated by the 3 s and 4 s orbitals of sulfur and selenium, whereas the far region of the conduction band (VB) is dominated by the s and p orbitals of platinum and selenium. This data provides the strongest support for the band structure results.

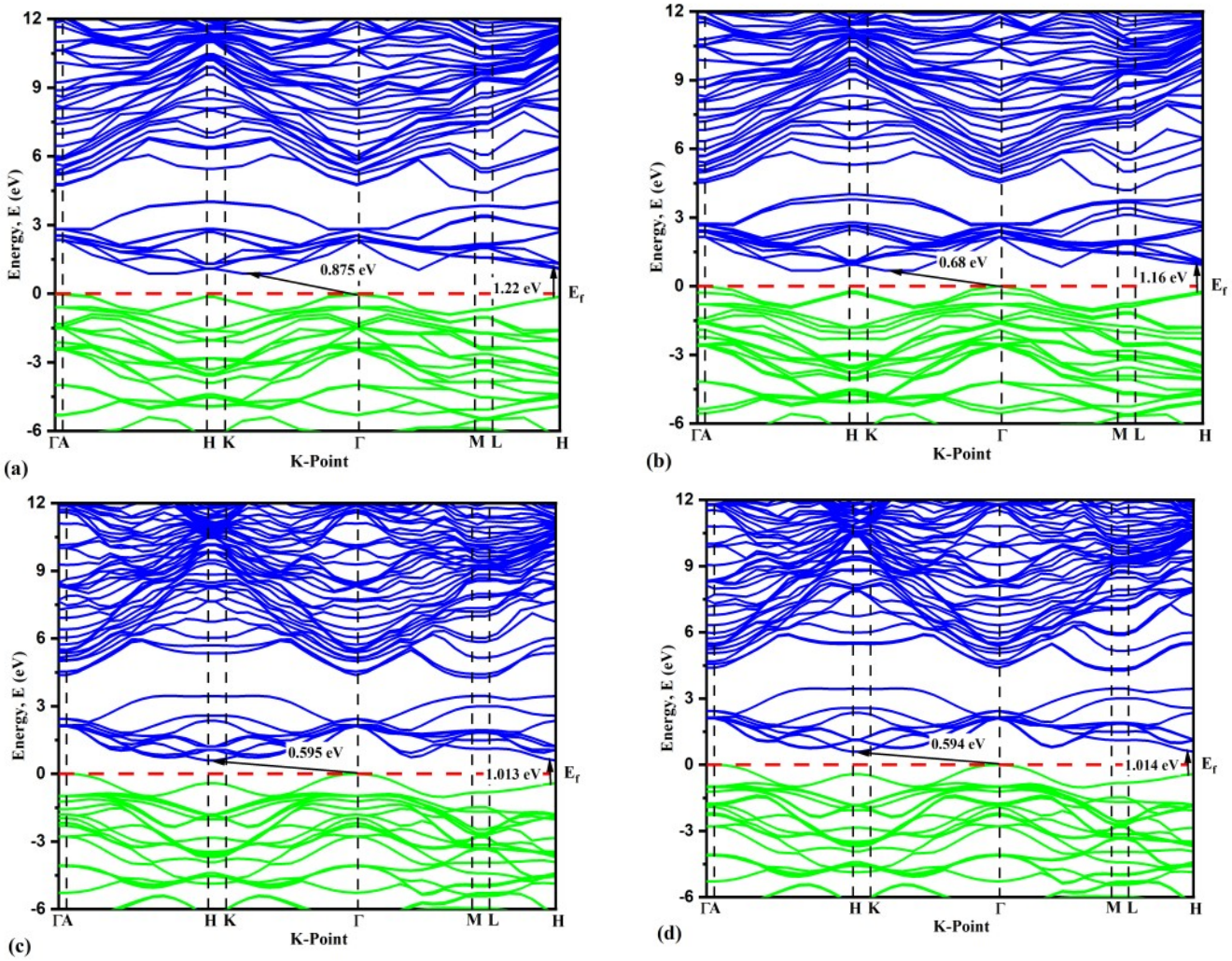

Figure 5: The band structure of trilayer heterostructures (a) ABA, (b) BAA, (c) ABB, (d) BAB orders.

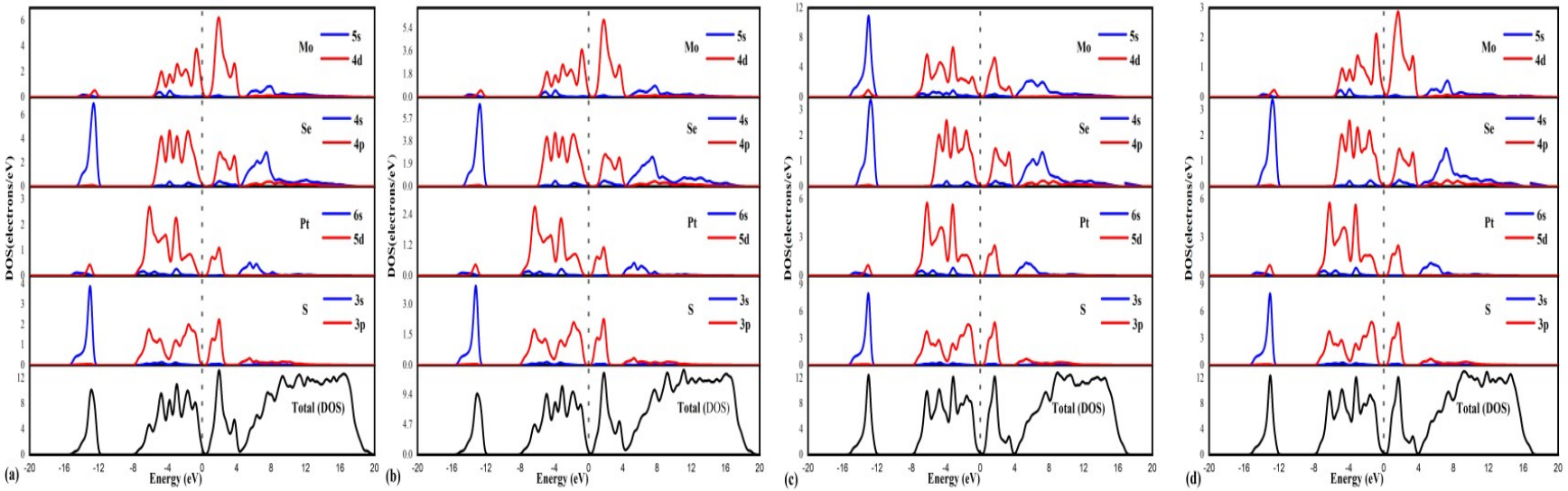

Figure 6: TDOS and PDOS of trilayer heterostructures (a) ABA, (b) BAA, (c) ABB, (d) BAB orders.

3.2. The Optical Properties

To determine the possible uses of a material in optical detection and electronic devices, its optical properties are crucial. Within the energy range of up to 30 eV, the optical properties of the layers were determined in the current study.

To employ a material in high-performance solar cells and other photovoltaic devices, it is necessary to understand its optical absorption, which offers essential information on how efficiently it transforms solar energy. The absorption coefficient (α) of trilayer heterostructures is illustrated in Fig. 7(a), After a careful analysis, we notice that the beginning of α in the infrared (IR) range, then, α increases with the growth of photon energy. This rise continues up to the highest value of α; 15.2×10^4, 15×10^4, 15×10^4, and 14.9×10^4 cm^{-1}, for ABB, ABA, BAA, and BAB orders, respectively, all these values are positioned in the ultraviolet region. To be precise, this does not mean neglecting the value of the absorption coefficient in other regions, as its value in the visible region is also very high and equal to 8×10^4 cm^{-1}. In addition, the absorption coefficient of the ABA and BAA have two peaks, not three as in ABB and BAB orders.

Reflectivity as a function of phonon energy is depicted in Fig. 7(b) Clearly, the static reflectivity of ABA, BAA, ABB, and BAB orders at zero energy is 22.5%, 22.2%, 21.9%, and 21.5%, respectively. However, the maximum values of reflectivity are 33.1% (ABA), 33% (BAA), 32.9% (ABB), and 32.7% (BAB); hence, the maximum values of reflectivity cannot exceed 33.1% for all trilayer vdW heterostructures. In addition, there are two peaks of reflectivity for ABA and BAA orders and three peaks for ABB and BAB orders, with the principal peaks for ABA, BAA, ABB, and BAB orders occurring in the visible range at energies of 2.67, 2.78, 2.78, and 2.67 eV, respectively. Reflectivity demonstrated a notable amount of anisotropy in the energy range of 0 to 21 eV, which decreases gradually to zero above 27 eV. Trilayer vdW heterostructures can therefore be used as coating nanomaterials in the visible and ultraviolet spectrum. The optical conductivity (σ) versus the photon energy of heterostructures described in Fig. 7(c) Clearly, there are two main peaks for ABA and BAA orders and three main peaks for ABB and BAB orders. Although the conductivity commences from the IR region, their main peaks are positioned at the end of the infrared region and the beginning of the visible light region. Precisely, the uppermost values of conductivity are 2.8, 2.77, 2.65, and 2.6, positioned at 1.6 eV for all orders. After about 13.5 eV, the optical conductivity begins to decrease with the growth of photon energy.

The real (Re ε) and imaginary (Im ε) components of the dielectric function are computed and depicted in Fig. 7(d) and (e). The results of the (Re ε) portion indicate that the topmost peaks of heterostructures are 9.66 (ABA), 9.58 (BAA), 9.45 (ABB), and 9.23 (BAB) at phonon energies of approximately 1.47 eV, 1.53 eV, 1.58eV, and 1.64eV, respectively. After about 21 eV, the (Re ε) part becomes constant. Generally, it is notable that the superior (Re ε) part is located in the visible region. In contrast, the results indicate that for all cases, the imaginary parts (Im ε) of the dielectric function have one maximum peak in visible light. Nevertheless, the (Re ε) and (Im ε) peaks of the dielectric function of ABA layers are always greater than those of other layers. These peaks demonstrate that there is no additional transition between the valence and conduction bands. Because the number of peaks increases or decreases with the amount of electron transitions, when the number of peaks increases, more electrons are transferred between the valence and conduction bands.

Materials' optoelectronic properties are substantially influenced by the refractive index. Fig. 7(f) depicts the refractive index as a function of phonon energy (f). At zero photon energy, the static refractive indices of the real part for the ABA, BAA, ABB, and BAB orders are 2.82, 2.80, 2.77, and 2.72, respectively. Additions For all trilayers, The maximum refractive index occurs near 2 eV, Beyond these values, the refractive index decreases gradually as photon energy increases. The refractive index remains constant after approximately 21 eV, In other words, after 21 eV, these heterostructures become anisotropic. These trilayers can be used as an internal layer coating between the substrate and ultraviolet absorbing layer due to their high refractive indices.

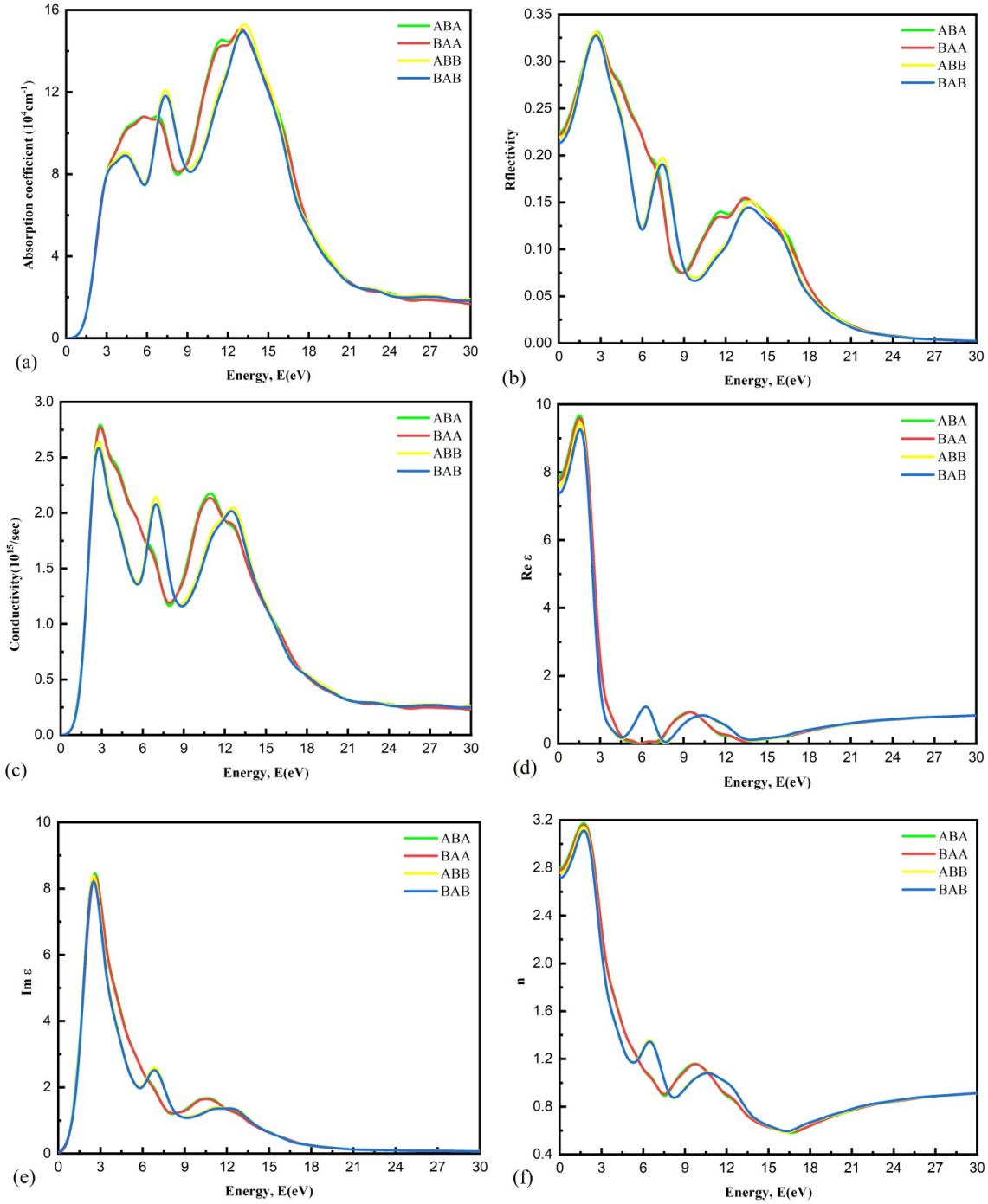

Figure 7: The optical characteristics of triple-layer heterostructures (a) the Absorption coefficient, (b) the reflectivity, (c) the conductivity, (d) the real part of the dielectric function, (e) the imaginary part of the dielectric function, (f) the refraction index.

4. CONCLUSIONS

In summary, we studied four orders of trilayer heterostructure. Using the PBE method the band gaps of All trilayers are between 0.594 to 0.875 eV, appealing for applications in nanoelectronics. Additionally, their direct energy gaps are nearly twice as great as their indirect energy gaps. On the other hand, it is found that the bandgaps of the trilayer heterostructures are much smaller than those in the monolayer counterpart. the VB and CB near the Fermi level are composed of the p orbitals of S and Se atoms and the d orbitals of Mo and Pt atoms. According to optical simulations, the absorption coefficient of these unique trilayer heterostructures is extremely high in the visible light spectrum. ABA and BAA orders have higher optical property values in lower energy regions

before 6 eV. Due to the unique optical and electronic features of trilayer vdW heterostructures, it is hypothesized that these heterostructures can be utilized in optoelectronics and nanoelectronics applications.

5. CONFLICT OF INTERESTS

The authors declare that they have no conflict of interests.

6. REFERENCES

1. Nandi P, Rawat A, Ahammed R, Jena N, De Sarkar A. Group-IV (A) Janus dichalcogenide monolayers and their interfaces straddle gigantic shear and in-plane piezoelectricity. Nanoscale. 2021;13(10):5460-78. Available from: <URL>.

2. Nguyen HT, Vu TV, Binh NT, Hoat D, Hieu NV, Anh NT, et al. Strain-tunable electronic and optical properties of monolayer GeSe: promising for photocatalytic water splitting applications. Chemical Physics. 2020;529:110543. Available from: <URL>.

3. Naguib M, Mochalin VN, Barsoum MW, Gogotsi Y. 25th anniversary article: MXenes: a new family of two-dimensional materials. Advanced materials. 2014;26(7):992-1005. Available from: <URL>.

4. Vogt P, De Padova P, Quaresima C, Avila J, Frantzeskakis E, Asensio MC, et al. Silicene: compelling experimental evidence for graphenelike two-dimensional silicon. Physical review letters. 2012;108(15):155501. Available from: <URL>.

5. Zhang Y, Ye H, Yu Z, Liu Y, Li Y. First-principles study of square phase MX2 and Janus MXY (M= Mo, W; X, Y= S, Se, Te) transition metal dichalcogenide monolayers under biaxial strain. Physica E: Low-dimensional Systems and Nanostructures. 2019;110:134-9. Available from: <URL>.

6. Liu C-C, Feng W, Yao Y. Quantum spin Hall effect in silicene and two-dimensional germanium. Physical review letters. 2011;107(7):076802. Available from: <URL>.

7. Li P, Appelbaum I. Symmetry, distorted band structure, and spin-orbit coupling of group-III metal-monochalcogenide monolayers. Physical Review B. 2015;92(19):195129. Available from: <URL>.

8. Ren C, Wang S, Tian H, Luo Y, Yu J, Xu Y, et al. First-principles investigation on electronic properties and band alignment of group III monochalcogenides. Scientific Reports. 2019;9(1):1-6. Available from: <URL>.

9. Koenig SP, Doganov RA, Schmidt H, Castro Neto A, Özyilmaz B. Electric field effect in ultrathin black phosphorus. Applied Physics Letters. 2014;104(10):103106. Available from: <URL>.

10. Zhu F-f, Chen W-j, Xu Y, Gao C-l, Guan D-d, Liu C-h, et al. Epitaxial growth of two-dimensional stanene. Nature materials. 2015;14(10):1020-5. Available from: <URL>.

11. Bassman L, Rajak P, Kalia RK, Nakano A, Sha F, Aykol M, et al. Efficient discovery of optimal N-layered TMDC hetero-structures. Mrs Advances. 2018;3(6-7):397-402. Available from: <URL>.

12. Flöry N, Jain A, Bharadwaj P, Parzefall M, Taniguchi T, Watanabe K, et al. A WSe2/MoSe2 heterostructure photovoltaic device. Applied Physics Letters. 2015;107(12):123106. Available from: <URL>.

13. Bastonero L, Cicero G, Palummo M, Re Fiorentin M. Boosted Solar Light Absorbance in PdS2/PtS2 Vertical Heterostructures for Ultrathin Photovoltaic Devices. ACS applied materials & interfaces. 2021;13(36):43615-21. Available from: <URL>.

14. Wu D, Li W, Rai A, Wu X, Movva HC, Yogeesh MN, et al. Visualization of local conductance in MoS2/WSe2 heterostructure transistors. Nano letters. 2019;19(3):1976-81. Available from: <URL>.

15. Soares DM, Mukherjee S, Singh G. TMDs beyond MoS2 for electrochemical energy storage. Chemistry–A European Journal. 2020;26(29):6320-41. Available from: <URL>.

16. Prabhu P, Jose V, Lee J-M. Design strategies for development of TMD-based heterostructures in electrochemical energy systems. Matter. 2020;2(3):526-53. Available from: <URL>.

17. Fan X, Li X, Zhao Z, Yue Z, Feng P, Ma X, et al. Heterostructured rGO/MoS2 nanocomposites toward enhancing lubrication function of industrial gear oils. Carbon. 2022;191:84-97. Available from: <URL>.

18. Feng P, Ren Y, Li Y, He J, Zhao Z, Ma X, et al. Synergistic lubrication of few-layer Ti3C2Tx/MoS2 heterojunction as a lubricant additive. Friction. 2022:1-15. Available from: <URL>.

19. Liu H, Huang Z, Wu G, Wu Y, Yuan G, He C, et al. A novel WS 2/NbSe 2 vdW heterostructure as an ultrafast charging and discharging anode material for lithium-ion batteries. Journal of Materials Chemistry A. 2018;6(35):17040-8. Available from: <URL>.

20. Pham KD, Hieu NN, Bui LM, Phuc HV, Hoi BD, Tu LT, et al. Vertical strain and electric field tunable electronic properties of type-II band alignment C2N/InSe van der Waals heterostructure. Chemical Physics Letters. 2019;716:155-61. Available from: <URL>.

21. Zhao X, Tang G, Li Y, Zhang M, Nie Y. Biaxial strain improving the thermoelectric performance of a two-dimensional MoS2/WS2 heterostructure. ACS Applied Electronic Materials. 2021;3(7):2995-3004. Available from: <URL>.

22. Xia C, Xiong W, Du J, Wang T, Peng Y, Li J. Universality of electronic characteristics and photocatalyst applications in the two-dimensional Janus transition metal dichalcogenides. Physical Review B. 2018;98(16):165424. Available from: <URL>.

23. Mak KF, Lee C, Hone J, Shan J, Heinz TF. Atomically thin MoS 2: a new direct-gap semiconductor. Physical review letters. 2010;105(13):136805. Available from: <URL>.

24. Imani Yengejeh S, Wen W, Wang Y. Mechanical properties of lateral transition metal dichalcogenide heterostructures. Frontiers of Physics. 2021;16(1):1-7. Available from: <URL>.

25. Dong R, Kuljanishvili I. Progress in fabrication of transition metal dichalcogenides heterostructure systems. Journal of Vacuum Science & Technology B, Nanotechnology and Microelectronics: Materials, Processing, Measurement, and Phenomena. 2017;35(3):030803. Available from: <URL>.

26. Datta K, Shadman A, Rahman E, Khosru QD. Trilayer TMDC heterostructures for MOSFETs and nanobiosensors. Journal of Electronic Materials. 2017;46(2):1248-60. Available from: <URL>.

27. Jin C, Ma EY, Karni O, Regan EC, Wang F, Heinz TF. Ultrafast dynamics in van der Waals heterostructures. Nature nanotechnology. 2018;13(11):994-1003. Available from: <URL>.

28. Naseri M. First-principles prediction of a novel cadmium disulfide monolayer (penta-CdS2): Indirect to direct band gap transition by strain engineering. Chemical Physics Letters. 2017;685:310-5. Available from: <URL>.

29. Lee YH, Zhang XQ, Zhang W, Chang MT, Lin CT, Chang KD, et al. Synthesis of large-area MoS2 atomic layers with chemical vapor deposition. Advanced materials. 2012;24(17):2320-5. Available from: <URL>.

30. Wang X, Gong Y, Shi G, Chow WL, Keyshar K, Ye G, et al. Chemical vapor deposition growth of crystalline monolayer MoSe2. ACS nano. 2014;8(5):5125-31. Available from: <URL>.

31. Yumigeta K, Brayfield C, Cai H, Hajra D, Blei M, Yang S, et al. The synthesis of competing phase GeSe and GeSe 2 2D layered materials. RSC advances. 2020;10(63):38227-32. Available from: <URL>.

32. Zhao D, Xie S, Wang Y, Zhu H, Chen L, Sun Q, et al. Synthesis of large-scale few-layer PtS2 films by chemical vapor deposition. AIP Advances. 2019;9(2):025225. Available from: <URL>.

33. Meng L, Xu C, Li H, Wang X, Yan X. Controlled synthesis and frictional properties of 2D MoTe2 via chemical vapor deposition. Chemical Physics Letters. 2019;728:156-9. Available from: <URL>.

34. Meng L, Hu S, Yan W, Feng J, Li H, Yan X. Controlled synthesis of large scale continuous monolayer WS2 film by atmospheric pressure chemical vapor deposition. Chemical Physics Letters. 2020;739:136945. Available from: <URL>.

35. Ghiasi TS, Quereda J, Van Wees BJ. Bilayer h-BN barriers for tunneling contacts in fully-encapsulated monolayer MoSe2 field-effect transistors. 2D Materials. 2018;6(1):015002. Available from: <URL>.

36. Han G, Kaniselvan M, Yoon Y. Photoresponse of MoSe2 transistors: A fully numerical quantum transport simulation study. ACS Applied Electronic Materials. 2020;2(11):3765-72. Available from: <URL>.

37. Xiong R, Hu R, Zhang Y, Yang X, Lin P, Wen C, et al. Computational discovery of PtS 2/GaSe van der Waals heterostructure for solar energy applications. Physical Chemistry Chemical Physics. 2021;23(36):20163-73. Available from: <URL>.

38. Chen C, Cao J, Yin W, Zhang Q, Yao Y, Wei X. Single transition metal atom modified MoSe2 as a promising electrocatalyst for nitrogen Fixation: A first-principles study. Chemical Physics Letters. 2021;780:138939. Available from: <URL>.

39. Liu G, Gan Y, Quhe R, Lu P. Strain dependent electronic and optical properties of PtS2 monolayer. Chemical Physics Letters. 2018;709:65-70. Available from: <URL>.

40. Wasey AA, Chakrabarty S, Das G. Substrate induced modulation of electronic, magnetic and chemical properties of MoSe2 monolayer. AIP Advances. 2014;4(4):047107. Available from: <URL>.

41. Clark SJ, Segall MD, Pickard CJ, Hasnip PJ, Probert MI, Refson K, et al. First principles methods using CASTEP. Zeitschrift für kristallographie-crystalline materials. 2005;220(5-6):567-70. Available from: <URL>.

42. Perdew JP, Burke K, Ernzerhof M. Generalized gradient approximation made simple. Physical review letters. 1996;77(18):3865. Available from: <URL>.

43. Vanderbilt D. Soft self-consistent pseudopotentials in a generalized eigenvalue formalism. Physical review B. 1990;41(11):7892. Available from: <URL>.

44. Monkhorst HJ, Pack JD. Special points for Brillouin-zone integrations. Physical review B. 1976;13(12):5188. Available from: <URL>.

45. Mir SH, Chakraborty S, Wärnå J, Narayan S, Jha PC, Jha PK, et al. A comparative study of hydrogen evolution reaction on pseudo-monolayer WS 2 and PtS 2: insights based on the density functional theory. Catalysis Science & Technology. 2017;7(3):687-92. Available from: <URL>.

46. Yao W, Guan H, Zhang K, Wang G, Wu X, Jia Z. Nb-doped PtS2 monolayer for detection of C2H2 and C2H4 in on-load tap-changer of the oil-immersed transformers: A first-principles study. Chemical Physics Letters. 2022:139755. Available from: <URL>.

47. Li Y, Feng Z, Sun Q, Ma Y, Tang Y, Dai X. Electronic, thermoelectric, transport and optical properties of MoSe2/BAs van der Waals heterostructures. Results in Physics. 2021;23:104010. Available from: <URL>.

48. Hu X, Zhang Q, Yu S. Theoretical insight into the hydrogen adsorption on MoS2 (MoSe2) monolayer as a function of biaxial strain/external electric field. Applied Surface Science. 2019;478:857-65. Available from: <URL>.

49. Wu Q, Fu X, Yang K, Wu H, Liu L, Zhang L, et al. Promoting a weak coupling of monolayer MoSe2 grown on (100)-faceted Au foil. ACS nano. 2021;15(3):4481-9. Available from: <URL>.

50. Zhang Y, Chang T-R, Zhou B, Cui Y-T, Yan H, Liu Z, et al. Direct observation of the transition from indirect to direct bandgap in atomically thin epitaxial MoSe2. Nature nanotechnology. 2014;9(2):111-5. Available from: <URL>.

51. Yadav VK, Kumar PP, Singh V. Effect of different precursors on morphology of CVD synthesized MoSe2. Materials Today: Proceedings. 2022;56:3786-9. Available from: <URL>.

52. Tao W-L, Mu Y, Hu C-E, Cheng Y, Ji G-F. Electronic structure, optical properties, and phonon transport in Janus monolayer PtSSe via first-principles study. Philosophical Magazine. 2019;99(8):1025-40. Available from: <URL>.